Formation and Properties of Reverse Micellar Cubic Liquid Crystals and Derived Emulsions

ARTICLE *in* LANGMUIR · NOVEMBER 2007

Impact Factor: 4.46 · DOI: 10.1021/la701722f · Source: PubMed

7 AUTHORS, INCLUDING:

Lok Kumar Shrestha
National Institute for Materials Science
109 PUBLICATIONS **1,416** CITATIONS

SEE PROFILE

A. Maestro
University of Barcelona
31 PUBLICATIONS **688** CITATIONS

SEE PROFILE

Formation and Properties of Reverse Micellar Cubic Liquid Crystals and Derived Emulsions

Carlos Rodríguez-Abreu,*,† Lok Kumar Shrestha,‡ Dharmesh Varade,‡ Kenji Aramaki,‡ Alicia Maestro,§ Arturo López Quintela,|| and Conxita Solans†

Institut d'Investigacions Químiques i Ambientals de Barcelona, Consejo Superior de Investigaciones Científicas (IIQAB/CSIC), Jordi Girona, 18-26, 08034 Barcelona, Spain, Graduate School of Environment and Information Sciences, Yokohama National University, Tokiwadai 79-7, Hodogaya-ku, Yokohama 240-8501, Japan, Department of Chemical Engineering, Barcelona University, Martı i Franques 1, 08028 Barcelona, Spain, and Departamento de Química Física, Facultad de Química, Universidad de Santiago de Compostela, E-15782 Santiago de Compostela, Spain

Received July 9, 2007. In Final Form: August 16, 2007

The structure of the reverse micellar cubic (I_2) liquid crystal and the adjacent micellar phase in amphiphilic block copolymer/water/oil systems has been studied by small-angle X-ray scattering (SAXS), rheometry, and differential scanning calorimetry (DSC). Upon addition of water to the copolymer/oil mixture, spherical micelles are formed and grow in size until a disorder−order transition takes place, which is related to a sudden increase in the viscosity and shear modulus. The transition is driven by the packing of the spherical micelles into a *Fd3m* cubic lattice. The single-phase I_2 liquid crystals show gel-like behavior and elastic moduli higher than 10^4 Pa, as determined by oscillatory measurements. Further addition of water induces phase separation, and it is found that reverse water-in-oil emulsions with high internal phase ratio and stabilized by I_2 liquid crystals can be prepared in the two-phase region. Contrary to liquid−liquid emulsions, both the elastic modulus and the viscosity decrease with the fraction of dispersed water, due to a decrease in the crystalline fraction in the sample, although the reverse emulsions remain gel-like even at high volume fractions of the dispersed phase. A temperature induced order−disorder transition can be detected by calorimetry and rheometry. Upon heating the I_2 liquid crystals, two thermal events associated with small enthalpy values were detected: one endothermic, related to the "melting" of the liquid crystal, and the other exothermic, attributed to phase separation. The melting of the liquid crystal is associated with a sudden drop in viscosity and shear moduli. Results are relevant for understanding the formation of cubic-phase-based reverse emulsions and for their application as templates for the synthesis of structured materials.

Introduction

Reverse discontinuous (micellar) cubic liquid crystals are soft materials consisting of discrete reverse aggregates (with hydrophilic nuclei) ordered in cubic symmetry. This particular arrangement makes micellar cubic liquid crystals isotropic and extremely viscous. In the sequence of mesophases, reverse discontinuous cubic liquid crystals are those which possess the larger packing parameter[1] and the most negative interfacial mean curvature, that is, concave toward the hydrophilic phase and convex toward the hydrophobic continuous phase (usually an organic solvent).

Thermotropic discontinuous cubic liquid crystals have been found in polyhydroxy amphiphiles and other star shaped molecules,[2] whereas lyotropic reverse micellar cubic liquid crystals are formed by a few amphiphilic systems (lipids and block copolymers)[3−5] that are highly hydrophobic and flexible enough to overcome packing constraints and give negative surface curvature. Since reverse micellar cubic liquid crystals contain an arrangement of hydrophilic nanodomains, they are potential candidates for the preparation of nanostructured materials and ordered nanoparticles[6] and for controlled release of active ingredients. Moreover, one can take advantage of their very high viscosity for the preparation and stabilization of reverse emulsions,[7] which have found applications in many fields.[8,9] Particularly, it will be advantageous to have a nanostructure between droplets, since in such a case the emulsion could be used as a template for the preparation of meso-macroporous materials.[10]

Contrary to their counterparts the direct micellar cubic phases (formed by direct micelles with hydrophobic nuclei), there are very few reports on the rheology of reverse micellar cubic phases[11] and their formation from the adjacent reverse micellar phase. While this paper was under review, Pouzot et al.[12] published an article on the rheology and structure of a reverse micellar cubic phase in the monolinolein/water/limonene system. This topic is relevant for the above-mentioned applications, since the synthesis

* To whom correspondence should be addressed. E-mail: craqci@cid.csic.es.

† Institut d'Investigacions Químiques i Ambientals de Barcelona.

‡ Yokohama National University.

§ Barcelona University.

|| Universidad de Santiago de Compostela.

(1) Israelachvili, J.; Mitchell, D. J.; Ninham, B. W. *J. Chem. Soc., Faraday Trans. 2* **1976**, *72*, 1525.

(2) Cheng, X.; Das, K.; Diele, S.; Tschierske, C. *Langmuir* **2002**, *18*, 6521.

(3) Seddon, J. M.; Robins, J.; Gulik-Krzywicki, T.; Delacroix, H. *Phys. Chem. Chem. Phys.* **2000**, *2*, 4485.

(4) Alexandridis, P.; Olsson, U.; Lindman, B. *Langmuir* **1996**, *12*, 1419.

(5) Rodríguez, C.; López-Quintela, M. A.; Uddin, M. H.; Aramaki, K. Kunieda, H. In *Block copolymers in nanoscience*; Lazzari, M., Liu, G., Lecommandoux, S., Eds.; Wiley-VCH: Weinheim, 2006; Chapter 17, pp 391−415.

(6) Rodríguez, C.; Lazzari, M.; Varade, D.; Kaneko, M.; Aramaki, K.; López-Quintela, M. A. *Colloid Polym. Sci.* **2007**, *285*, 673.

(7) Uddin, M. H.; Rodríguez, C.; Watanabe, K.; López-Quintela, A.; Kato, T.; Furukawa, H.; Harashima, A.; Kunieda, H. *Langmuir* **2001**, *17*, 5169.

(8) Solans, C.; Esquena, J.; Azemar, N. *Curr. Opin. Colloid Interface Sci.* **2003**, *8*, 156.

(9) Solans, C.; Esquena, J.; Azemar, N.; Rodríguez, C.; Kunieda, H. In *Emulsions: Structure, Stability and Interactions*; Petsev, D., Ed.; Elsevier: Amsterdam, 2004; Chapter 13, pp 511−556.

(10) Esquena, J.; Solans, C. In *Emulsions and Emulsion Stability*; Sjoblom, J., Ed.; Taylor & Francis: Boca Raton, FL, 2006.

(11) Rodríguez, C.; Aramaki, K.; Kunieda, H. *Colloids Surf., A* **2005**, *269*, 59.

(12) Pouzot, M.; Mezzenga, R.; Leser, M.; Sagalowicz, L.; Guillot, S.; Glatter, O. *Langmuir* **2007**, *23*, 9618.

10.1021/la701722f CCC: $37.00
Published on Web 10/02/2007

and properties of materials usually depend on their micro- and nanostructure.

Here, we present a study on the formation and properties of reverse micellar cubic liquid crystals in a poly(ethylene oxide)−poly(propylene oxide)−poly(ethylene oxide) amphiphilic block copolymer/water/oil system, whose phase diagram was published previously.[13] There is an earlier report on the structure of a reverse micellar solution in PEO−PPO−PEO copolymers as a function of copolymer concentration.[14] However, we take a different approach and follow the structural changes as a function of added water, which is known to induce block segregation.[15] We have characterized the adjacent reverse micellar phase and the liquid crystals by small-angle X-ray scattering, rheometry, and differential scanning calorimetry. Moreover, the formation of highly internal-phase-ratio reverse emulsions (HIPRE) from the liquid crystals is also reported. This report is a part of a wider study on the preparation of porous materials using reverse concentrated emulsions as templates.

Experimental Section

Materials. The poly(ethylene oxide)−poly(propylene oxide)−poly(ethylene oxide) (PEO−PPO−PEO) triblock copolymer Pluronic L121 was obtained from BASF Corporation. The copolymer molecular formula can be represented as $EO_5PO_{68}EO_5$. *p*-Xylene (99%) was provided by Sigma-Aldrich. All substances were used without further purification. Deionized water was used in the measurements.

Methods. *Sample Preparation.* Single-phase samples (O_m or I_2) were prepared by weighing the appropriate amounts of the components in glass ampules with a narrow constriction. The ampules were flame-sealed immediately, and the samples were homogenized by using a vortex device and by repeated centrifugation in both directions. The ampules were then equilibrated in a temperature-controlled bath at 25 °C for several days.

Emulsions (in the two-phase region) were prepared by weighing the components in test tubes (inner diameter = 1 cm) with screw caps and then heating them at 60 °C for 5 min. Afterward, the samples were homogenized for 2 min using a vortex mixer Genie 2 at maximum speed and then kept in a thermostatic bath at 25 °C for 1 h before the measurements.

Small-Angle X-ray Scattering (SAXS). SAXS measurements were carried out using a SAXSess camera (Anton Paar, Austria) attached to a PW3830 laboratory X-ray generator with a long fine focus sealed glass X-ray tube (Kα wavelength of 0.1542 nm) (PANalytical) and operated at 40 kV and 50 mA. Focusing multiplayer optics and a block collimator provided an intense and monochromatic primary beam with low background. Samples were filled into a vacuum tight thin quartz capillary, and the reusable capillary was used for all measurements to attain exactly the same scattering volume and background contribution. The scattered intensities were recorded with an imaging plate (IP) detection system, Cyclone (Perkin-Elmer), and, via SAXSQuant software (Anton Paar), two-dimensional intensity data were converted to one-dimensional scattered intensities as a function of the magnitude of the scattering vector

$$q = \frac{4\pi}{\lambda}\sin(\theta/2) \tag{1}$$

where θ is the angle between the incident beam and the scattered radiation. Owing to a translucent beam stop, a measurement of an attenuated primary intensity at $q = 0$ can easily be done as a routine. Data were then accurately transmission-calibrated by normalizing the attenuated primary intensity at $q = 0$ to unity and were corrected for the background scattering from the capillary and the solvents. Using water as a secondary standard, data were converted into absolute scale.

Using the scattering vector, q^*, corresponding to the position of each reflection, we determined the Bragg spacing, d, of the liquid crystalline phases according to

$$d = \frac{2\pi}{q^*} \tag{2}$$

The characterization of the reverse micelles was made with the help of the generalized indirect fourier transformation (GIFT) technique, and the effect of added water was systematically studied. For monodisperse spherical particle systems, the total scattered intensity, $I(q)$, can generally be given by

$$I(q) = nP(q)\,S(q) \tag{3}$$

where $P(q)$ represents the single particle scattering contribution, called the form factor, and $S(q)$ is the static structure factor describing the interparticle scattering contribution. The relation given by eq 3 is true only for a monodisperse spherical system. However, it can be extended to polydisperse and elongated particle systems up to certain theoretical and practical limit.[16−18] The pair−distance distribution function $p(r)$ is related to $P(q)$ by a Fourier transformation as

$$P(q) = 4\pi\int_0^\infty p(r)\frac{\sin qr}{qr}\,\mathrm{d}r \tag{4}$$

The $p(r)$ value extracted from the experimental SAXS intensities allows us to evaluate the geometry of the scattering objects, involving the overall shape, size, and internal structure.

$S(q)$, describing the spatial distribution of the particles, is given by the Fourier transformation of the total correlation function, $h(r) = g(r) - 1$, as

$$S(q) = 1 + 4\pi n\int_0^\infty [g(r) - 1]r^2\,\frac{\sin qr}{qr}\,\mathrm{d}r \tag{5}$$

$S(q)$ is unity for ideally dilute systems.

Analysis of the SAXS data is usually done either by a model-independent approach or by direct modeling.[19] The model-independent approach method consist of an inverse Fourier transformation of the experimental scattering curve, which provides the pair−distance distribution function. The inverse Fourier transformation is usually done by the indirect Fourier transformation (IFT) method introduced by Glatter.[20,21] This method can be applied for all the systems for which the correlations have a finite range. However, IFT does not consider interparticle interactions, and hence, its use is limited to the dilute systems for which the particle interactions are considered to be negligible. In concentrated systems, the particle interactions come into play and one has to consider a proper structure factor model in the analysis of the SAXS data. In such systems, the use of the updated version of IFT (the generalized indirect fourier transformation (GIFT) approach) can be useful for the structural elucidation of the self-assemblies. In the present investigation, the SAXS data for the reverse micellar solutions were analyzed for $q = 0.08-5\ \mathrm{nm}^{-1}$ using the GIFT method,[22,23] which determines $P(q)$ and $S(q)$ simultaneously, using the combination of the model-free description for $P(q)$ and the modeled interparticle interaction potential and closure for $S(q)$. The detailed theoretical description on the method has been reported elsewhere.[24−28] In the present study, we employed the averaged structure factor model of a hardsphere (HS)

(13) Svensson, B.; Olsson, U.; Alexandridis, P. *Langmuir* **2000**, *16*, 6839.
(14) Svensson, B.; Olsson, U.; Alexandridis, P.; Mortensen, K. *Macromolecules* **1999**, *32*, 6725.
(15) Wu, G.; Zhou, Z.; Chu, B. *Macromolecules* **1993**, *26*, 2117.
(16) Shrestha, L. K.; Sato, T.; Acharya, D. P.; Iwanaga, T.; Aramaki, K.; Kunieda, H. *J. Phys. Chem. B* **2006**, *110*, 12266.
(17) Shrestha, L. K.; Sato, T.; Aramaki, K. *J. Phys. Chem. B* **2007**, *111*, 1664.
(18) Shrestha, L. K.; Sato, T.; Aramaki, K. *Langmuir* **2007**, *23*, 6606.
(19) Pedersen, J. S. *Adv. Colloid Interface Sci.* **1997**, *70*, 171.
(20) Glatter, O. *J. Appl. Crystallogr.* **1977**, *10*, 415.
(21) Glatter, O. *J. Appl. Crystallogr.* **1980**, 13, 577.
(22) Brunner, P. J.; Glatter, O. *J. Appl. Crystallogr.* **1997**, *30*, 431.
(23) Weyerich, B.; Brunner-Popela, J.; Glatter, O. *J. Appl. Crystallogr.* **1999**, *32*, 197.

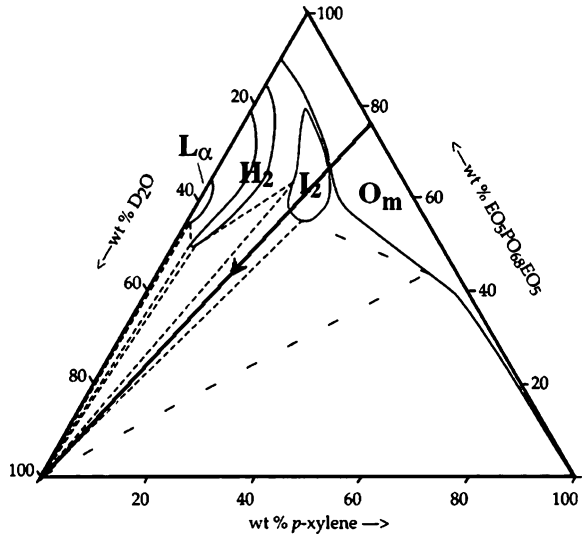

Figure 1. Phase diagram of the $EO_5PO_{68}EO_5/D_2O/p$-xylene system at 25 °C adapted from ref 12. Solid lines indicate the boundaries of the different one-phase regions, and broken lines indicate the three-phase triangles. The phases are as follows: L_α, lamellar; H_2, reverse hexagonal; I_2, reverse micellar cubic; and O_m, reverse micellar solution or copolymer molecular solution. The arrow represents the water-addition path followed in the present study.

interaction, $S(q)^{av}$,[29,30] and a Percus−Yevick (PY) closure to obtain analytical solutions of the Ornstein−Zernike (OZ) equation for the calculation of $h(r)$.

The electron density contrast profiles $\Delta\rho(r)$ (included in the Supporting Information), which reveal the inner structure of the scattering particles, were obtained from the $p(r)$ function by a convolution square root operation utilizing the DECON program.[31−33]

Rheometry. The rheological measurements were performed in a stress-controlled rheometer RS150 (Haake) using cone−plate or plate−plate geometry with the plate temperature being controlled by a TC501 (Haake) unit. A sample cover which sits over the geometry (but does not touch it) and is soaked with the solvent so that the space around the sample becomes saturated with the solvent vapor was used to minimize the change in sample composition by evaporation during the measurements. Frequency sweep measurements were performed in the linear viscoelastic regime of the samples, as determined previously by dynamic strain sweep measurements. The zero-shear viscosity of the samples was determined by extrapolating the viscosity-shear-rate curve to the zero-shear rate.

Differential Scanning Calorimetry (DSC). A differential scanning microcalorimeter (Setaram Micro DSC III) was used. The samples (300 mg) were introduced in Hastelloy pans. DSC traces were recorded using a heating rate of 1.5 °C/min under nitrogen atmosphere. An empty pan was used as a reference.

Optical Microscopy. Digital images were acquired with a Reichert Polyvar 2 (Leica) microscope equipped with video, polarizers, and an interference contrast prism.

Results and Discussion

SAXS Measurements. Figure 2 shows the desmeared SAXS patterns for the $EO_5PO_{68}EO_5/p$-xylene/water samples along the water addition path shown in Figure 1. The strong q dependence of the scattered intensity reveals the presence of aggregates. Moreover, the well-defined correlation peaks are indicative of interactions among aggregates. Those interactions become stronger as water is added to the system, as reflected by an increase in the peak intensity. The peaks also shift to lower q values as the water concentration is increased, suggesting longer distances between aggregates. It should be pointed out that the scattering intensity was very low in the absence of water. Hence, the hydration of PEO chains appears to be necessary for the formation of definite aggregates.

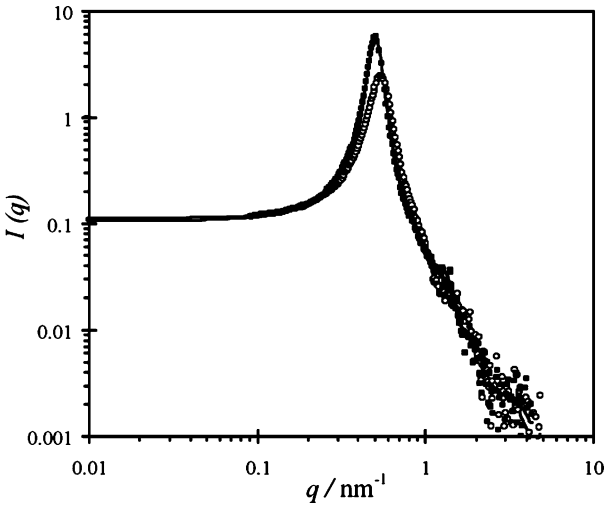

Figure 2. Desmeared SAXS patterns for $EO_5PO_{68}EO_5$/water/p-xylene samples at $\phi_w = 0.05$ (open symbols) and $\phi_w = 0.10$ (filled symbols). The $EO_5PO_{68}EO_5/p$-xylene weight ratio is 77/23. The lines are best fits using GIFT analysis.

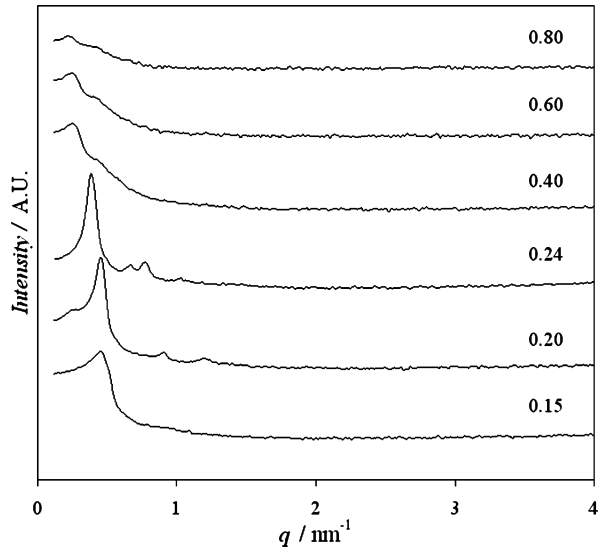

Figure 3. SAXS patterns of the $EO_5PO_{68}EO_5$/water/p-xylene system. The labels above each curve indicate the volume fraction of water (ϕ_w) in the samples. The $EO_5PO_{68}EO_5/p$-xylene weight ratio is fixed at 77/23. The curves were multiplied by arbitrary factors for clarity of presentation.

SAXS patterns at higher water contents are presented in Figure 3. The samples at $\phi_w = 0.2$ and 0.24 show several resolved peaks, corresponding to liquid crystalline samples with long-range order. The number and intensity of the reflections decrease with water content in the two-phase region ($\phi_w > 0.24$), since the fraction of liquid crystal in the sample is decreasing. Still,

(24) Sato, T.; Hossain, Md. K.; Acharya, D. P.; Glatter, O.; Chiba, A.; Kunieda, H. *J. Phys. Chem. B* **2004**, *108*, 12927.
(25) Acharya, D. P.; Sato, T.; Kaneko, M.; Singh, Y.; Kunieda, H. *J. Phys. Chem. B* **2006**, *110*, 754.
(26) Strey, R.; Glatter, O.; Schubert, K.-V.; Kaler, E. W. *J. Chem. Phys.* **1996**, *105*, 1175.
(27) Glatter, O. *Prog. Colloid Polym. Sci.* **1991**, *84*, 46.
(28) Fritz, G.; Bergmann, A. *J. Appl. Crystallogr.* **2004**, *37*, 815.
(29) Pusey, P. N.; Fijnaut, H. M.; Vrijm, A. *J. Chem. Phys.* **1982**, *77*, 4270.
(30) Salgi, P.; Rajagopolan, R. *Adv. Colloid Interface Sci.* **1993**, *43*, 169.
(31) Glatter, O. *J. Appl. Crystallogr.* **1981**, *14*, 101.
(32) Glatter, O.; Hainisch, B. *J. Appl. Crystallogr.* **1984**, *17*, 435.
(33) Mittelbach, R.; Glatter, O. *J. Appl. Crystallogr.* **1998**, *31*, 600.

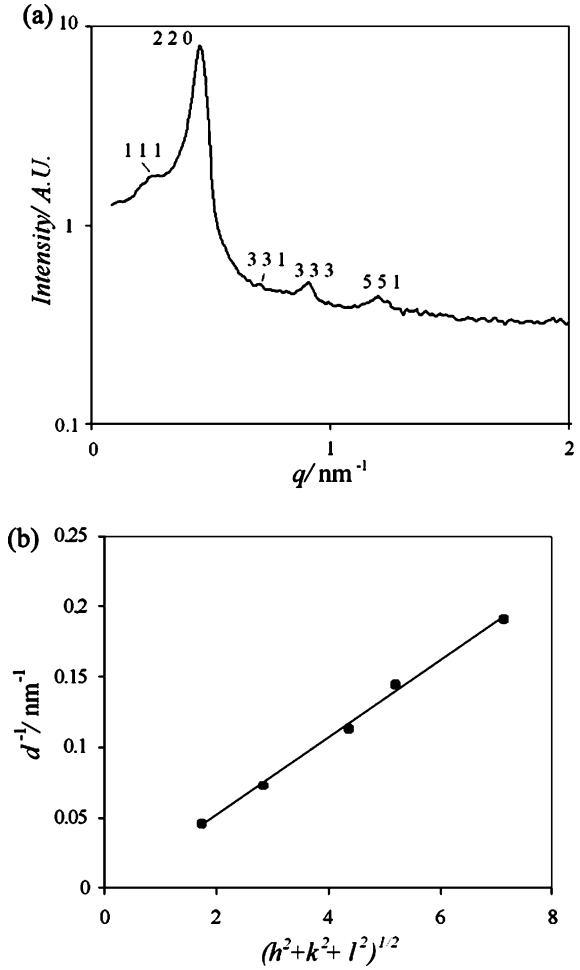

Figure 4. (a) SAXS pattern of a reverse micellar cubic phase (ϕ_w = 0.20, $EO_5PO_{68}EO_5$/*p*-xylene = 77/23) and (b) indexing of the peaks indicated in (a). The line is a best fit.

correlation peaks can be identified even at $\phi_w = 0.80$ in emulsified samples. Namely, the emulsions contain an ordered phase surrounding the droplets, as will be described later. Note that the position of the main peak is unchanged in the two-phase region ($\phi_w > 0.24$), since the micelles are saturated with water and do not swell anymore.

In all cases, broad peaks were observed (data not shown) in the wide-angle range (high q) at around $q = 14\ nm^{-1}$, which can be assigned to the hydrated poly(oxyethylene) chains in a disordered (liquid-like) state, with no short-range order.

As can be seen in Figure 4a, five peaks can be resolved from the SAXS pattern at $\phi_w = 0.20$ corresponding to the diffraction planes [111], [220], [331], [333], and [551] of the face-centered space group, *Fd*3*m*. This assignment has been suggested previously for the same system, although from a less resolved pattern.[13] The face-centered array is typical of systems with short-range interactions[34]that might be favored by the fact that PPO chains covering the surface of reverse micelles in solvents such xylene are in a back folded configuration, since the solvent becomes poorer for PPO chains as water is added.[35]

The indexing of the peaks is obtained from the plot of $1/d$ versus $(h^2 + k^2 + l^2)^{1/2}$ giving a straight line passing through the origin of the coordinates (Figure 4b). From the inverse of the slope, the unit cell parameter is estimated to be 44 nm. The

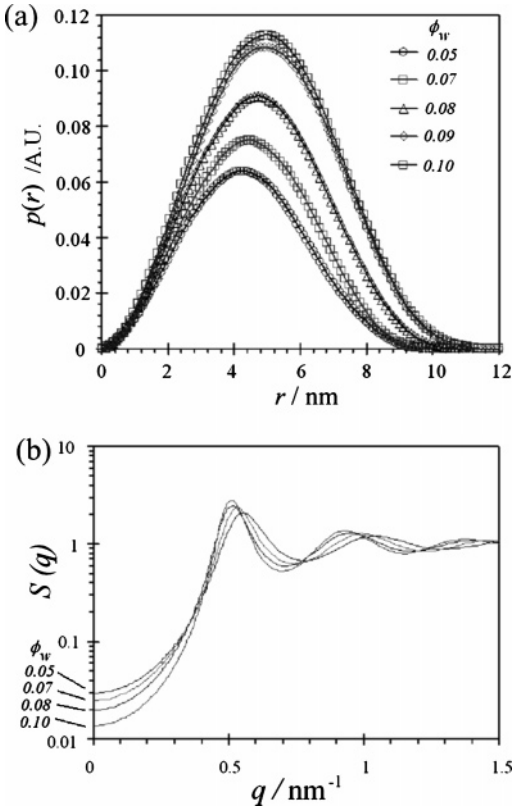

Figure 5. (a) Pair−distance distribution functions, $p(r)$, of EO_5-$PO_{68}EO_5$/water/*p*-xylene containing different volume fractions of solubilized water and (b) hard-sphere structure factors. The EO_5-$PO_{68}EO_5$/p-xylene ratio is 77/23.

radius of the hydrophilic micellar core in the cubic phase can be calculated as

$$r_c = \left(\frac{3(\phi_{EO} + \phi_w)}{4\pi N}\right)^{1/3} a \qquad (6)$$

where ϕ_{EO} and ϕ_w are the volume fractions of EO chains and water in the system, respectively, a is the unit cell parameter, and N is the number of micelles per unit cell. Using the structure for the reverse cubic phase of *Fd*3*m* proposed by Seddon,[36] that is, one consisting of 24 micelles per unit cell, the radius of the micellar core is calculated to be 6 nm at $\phi_w = 0.20$. We should point out that eq 6 is derived for micelles of the same size, which is a simplification compared to the model of Seddon consisting of two types of micelles.

Results from GIFT analysis of SAXS data in the O_m region are presented in Figure 5. As can be seen in Figure 5a, the pair−distance distribution functions are symmetric irrespective of the water content, indicating that the aggregates are spherical within the O_m phase. It should be mentioned that the existence of the cubic face-centered structure at higher water contents indirectly suggests that packed micelles have an almost spherical shape (ordering is expected to occur in monodisperse spherical systems having repulsive interactions[34]), which supports the GIFT analysis. The position of the maximum, which gives an estimation of the micellar radius (r_{mic}), shifts to higher r values as the water content increases; that is, the micelles swell with water. The electron density difference (i.e., contrast) seems to not be enough to resolve a core−shell structure of the micelles.

(34) Gast, A. P. *Langmuir* **1996**, *12*, 4060.
(35) Zhou, S.; Su, J.; Chu, B. *J. Polym. Sci., Part B: Polym. Phys.* **1998**, *36*, 889.
(36) Seddon, J. M.; Bartle, E. A.; Mingins, J. *J. Phys.; Condens. Matter* **1990**, *2*, SA285.

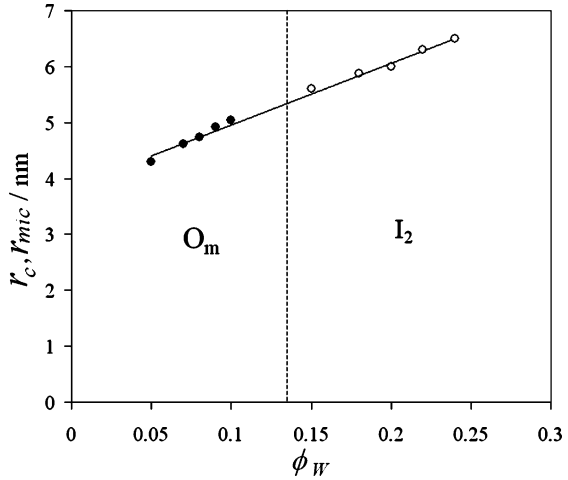

Figure 6. Micellar radius as derived from the pair−distance distribution functions, r_{mic} (filled symbols), and from eq 6, r_c (open symbols), as a function of the volume fraction of water ϕ_w. The line is a visual guide.

The structure factor profiles (Figure 5b) reveal the presence of considerable intermicellar interactions, which are responsible for the peaks shown in Figure 2. The micellar swelling is reflected in the shift of the structure factor peaks to smaller q values. On the other hand, the increase in the amplitude of the peaks indicates an increase in the volume fraction of the scattering entities. The $S(0)$ value decreases with the concentration of water, reflecting the decreasing mean distance between the neighboring micelles and, hence, the osmotic compressibility. At higher q values, all the curves converge to unity, since at length scales smaller than the dimensions of the scattering entities interparticle interactions are not relevant. The actual structure factor peaks might differ from what is predicted for monodisperse hard spheres.[14] Apart from polydispersity effects, some differences could arise due to a pair interaction softer than that predicted by the used hard-sphere model.[34] In any case, the polydispersity derived from the fittings to the present experimental data was low (around 0.05). In the range of water concentrations shown in Figure 5a, the hard-sphere volume fraction changed from 0.43 to 0.51, which is still below the random close-packed limit (0.64).

The values of r at the maximum of the $p(r)$ functions in Figure 5a, denoted as r_{mic}, are plotted as a function of water content in Figure 6. Data on the micellar core radius in the I_2 phase, calculated from eq 6, are also included for comparison. Svensson et al.[14] used a core−shell model to estimate the structural parameters of reverse micelles of PEO−PPO−PEO block copolymers of different EO chain lengths in a water/xylene mixture, using small-angle neutron scattering (SANS) measurements. We plotted their data for the radius of the micellar core at $\phi_w = 0.04$ as a function of EO chain length (see the Supporting Information) and made an extrapolation to the present case (EO chain = 5 units), obtaining a radius of 4 nm for the hydrophilic core, in close agreement with the results shown in Figure 6. This suggests that the pair−distance distribution functions of Figure 5a are reflecting mostly the contribution of the cores to the scattering, due to low contrast between the PPO chains and the solvent (*p*-xylene), as mentioned above. This was confirmed by calculating the radial electron density profile, $\Delta\rho_s(r)$, in which only the hydrophilic core with positive electron density difference could be resolved (see the Supporting Information).

On the other hand, there is no apparent discontinuity in the micellar radius when passing the O_m-I_2 phase boundary, which indicates that the reverse cubic phase seems to be formed by the packing of reverse micelles without any drastic dimensional change. Moreover, the similar trend in both the O_m and I_2 phases suggests that the GIFT results are reasonable, even though the copolymer concentration is quite high. To give additional support to the calculations, we attempted to use freeze fracture electron microscopy on the I_2 samples. Although it was not possible to clearly resolve the structure and crystalline planes (see the Supporting Information), it was clear that discrete aggregates with diameters around 10−15 nm were present (at $\phi_w = 0.20$), the values being close to the sizes derived from SAXS measurements. The estimated hard-core radius obtained from SAXS might be smaller than the actual size of the micelles due to a decreased center-to-center distance between micelles and an underestimated volume fraction due to an increased osmotic compressibility with an adhesive interaction between micelles.[6,37]

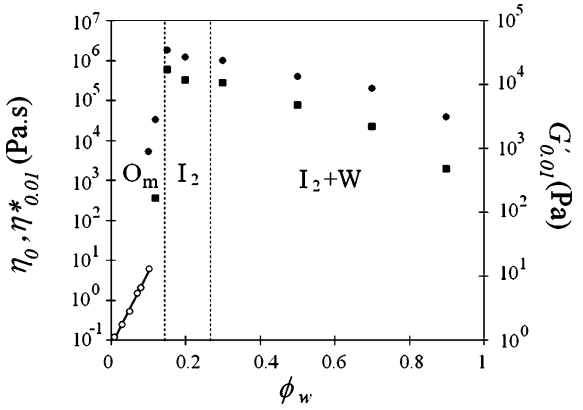

Figure 7. Zero-shear viscosity (open circles), $\eta^*_{0.01}$ ($\omega = 0.01\ s^{-1}$) (filled circles), and $G'_{0.01}$ ($\omega = 0.01\ s^{-1}$) (filled squares) as a function of the volume fraction of water in $EO_5PO_{68}EO_5$/*p*-xylene/water systems. The $EO_5PO_{68}EO_5$/*p*-xylene weight ratio is 77/23. W indicates excess water. Other notations are as those in Figure 1. The line is the best fit to the data for zero-shear viscosity.

Rheometry and Differential Scanning Calorimetry Measurements. Figure 7 shows rheometry results for $EO_5PO_{68}EO_5$/*p*-xylene/water systems. Samples in the reverse micellar solution region (O_m) were Newtonian. Above $\phi_w = 0.10$, there was no viscosity plateau at low frequencies (or low shear), and therefore, it was not possible to estimate η_o. In this case, the complex viscosity at a low frequency ($\omega = 0.01\ s^{-1}$) abbreviated as $\eta^*_{0.01}$ is shown as a reference. Similarly, values of the elastic modulus at low frequencies ($\omega = 0.01\ s^{-1}$) are presented in Figure 7. The viscosity increases as water is added to the $EO_5PO_{68}EO_5$/*p*-xylene mixture. This increase becomes suddenly sharp in the vicinity of the disorder−order transition ($O_m \rightarrow I_2$), with a jump in viscosity of 5 orders of magnitude from $\phi_w = 0.08$ to 0.15, indicating the criticality of the transition.[38] The change of viscosity in the O_m region (adjacent to the I_2 domain) follows an exponential trend with water concentration, similar to what was found recently for concentrated reverse micellar solutions in a graft copolymer system.[6] Although the experimental data are not enough for a further analysis, we attempted to make a qualitative (but cautious) comparison with some star copolymers in solution, which behave according to[39]

$$\eta_o = \eta_s \exp(bc^{\upsilon}) \qquad (7)$$

where η_s is the solvent viscosity, c is the polymer concentration, and b and υ are empirical constants. For a theta solvent,[39] $\upsilon = 0.8-1$. The exponential trend in Figure 7 would give $\upsilon = 1$. Such

(37) Singh-Zocchi, M.; Andreasen, A.; Zocchi, G. *Proc. Natl. Acad. Sci. U.S.A.* **1999**, *96*, 6711.
(38) Higgins, J. S.; Blake, S.; Tomlins, P. E.; Ross-Murphy, S. B.; Staples, E.; Penfold, J.; Dawkins, J. V. *Polymer* **1988**, *29*, 1968.
(39) Phillies, G. D. J.; Peczak, P. *Macromolecules* **1998**, *21*, 214.

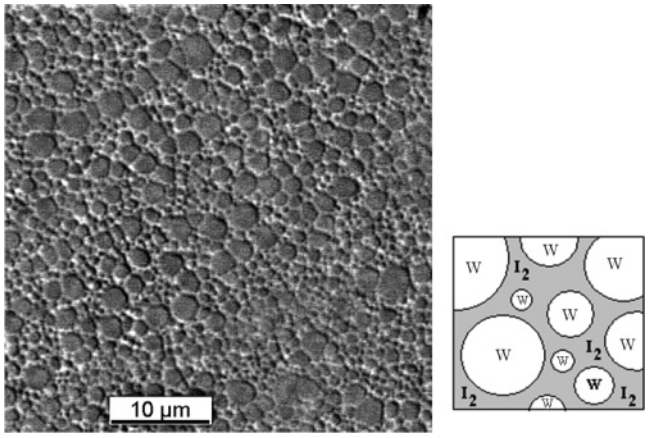

Figure 8. Image of a reverse emulsion stabilized by the I_2 phase ($EO_5PO_{68}EO_5$/*p*-xylene = 77/23) containing 90 vol % water. A schematic of the emulsion structure, with water droplets surrounded by the reverse cubic phase, is shown on the right.

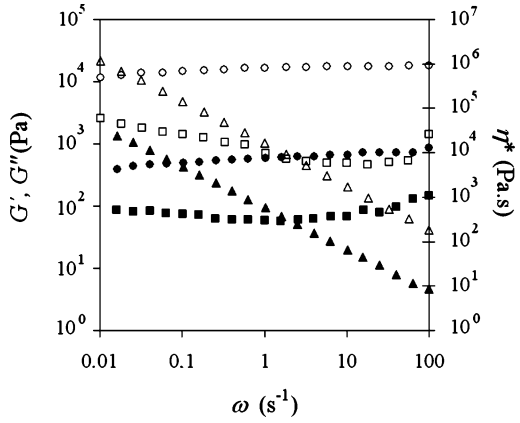

Figure 9. Dynamic rheometry data for $EO_5PO_{68}EO_5$/*p*-xylene/water systems. G' (circles), G'' (squares), and η^* (triangles) are the viscous modulus, the elastic modulus, and the complex viscosity, respectively. The $EO_5PO_{68}EO_5$/*p*-xylene ratio is 77/23, and the water volume fractions are 0.20 (open symbols) and 0.90 (filled symbols).

a trend is also in agreement with the Doolittle equation (based on excluded volume effects),[40]which was found to describe the temperature dependence of liquids approaching the glass transition.[41] One should be aware, however, of the significant differences between micelles and star polymers regarding relaxation phenomena and concentration regimes.

The onset of viscosity increase is indicative of the transition to the close packed system. Short-range adhesive interactions between particles together with chain interpenetration tend to shift the packing concentration toward values higher than that of hard spheres because adhesion creates additional space for particles to move in, owing to the formation of clusters of aggregates. Hence, the system can relax stress through restructuring of the micelles, preventing structural arrest.[42,43]

Upon further addition of water, phase separation takes place, and the reverse cubic phase coexists with excess water. It was found that reverse emulsions (containing dispersed water) based in the I_2 phase can be prepared in the I_2 + W region. A photomicrograph of such an emulsion containing 90 vol % water is shown in Figure 8. The emulsion is polydisperse in size, with some of the water droplets appearing as polyhedra, since the theoretical maximum volume fraction for random packing spheres has been surpassed. Some very small droplets (less than 1 μm) can also be observed, which also facilitates the close packing. The obtained emulsions are very stable, since the extremely high viscosity of the I_2 phase (acting as the external continuous phase) prevents droplet coalescence and creaming.[7,44]

Figure 9 shows the results on dynamic rheometry for selected samples in the I_2 and I_2 + W regions. There is no cross point between the elastic (G') and viscous (G'') moduli, indicating very long relaxation times, and the viscosity decreases monotonically with frequency (strong shear thinning), typical of systems having a yield stress, that is, gel-like behavior.[45,38] The G' values at $\phi_w = 0.20$ are above 10^4 Pa, which is typical for cubic phases.[12,46,47] The values of G', G'', and η^* tend decrease as water is added above the phase separation limit, that is, in the two-phase region (see Figure 7), but still remain very high up to $\phi_w = 0.90$. Moreover, little change was observed in the rheological behavior after aging the samples for weeks, indicating the high stability of the obtained emulsions.

The rheological behavior of cubic-phase-based emulsions (in the two-phase region) is opposite of that usually found in two-liquid-concentrated emulsions, in which stress moduli and viscosity increase with water content.[48,49] If it is considered that the structural units of the cubic phase form an elastic network, the elastic modulus would be proportional to the number of such units in the sample,[50] and then the viscosity will decrease with the cubic phase fraction in the system. Namely, the viscosity of the cubic-phase-based emulsions is mainly determined by the structured cubic phase. This behavior is similar to that found for the emulsions prepared from the direct micellar cubic phases.[47]

The fitting of G' versus ω data gives a power law $G' \approx \omega^{\Delta}$, where ω is the frequency. In the soft glass rheology (SRG) model,[51] the exponent Δ is related to an effective temperature x that originates from the interactions between the different entities. Below the glass transition, $x < 1$. Above the glass transition and for $1 < x < 3$, $G' \approx \omega^{x-1}$. When $x > 3$, $G' \approx \omega^2$ and the system behaves according to the Maxwell model. For the studied samples, $0 < \Delta < 1.2$; hence, the behavior is non-Maxwellian, suggesting multiple relaxation times. The values of Δ are plotted in Figure 10 as a function of water content. Δ decreases as water is added and finally becomes close to zero (i.e., G' is practically frequency independent) for the reverse micellar cubic phase at $\phi_w > 0.15$, indicating glassy-like behavior and dynamic "freezing" of the system. The value of the exponent Δ (0.73) at the onset of the disorder−order transition ($\phi_w \approx 0.10$) is not so far from that predicted by percolation theories, that is, 0.7.[52,53]

As shown in Figure 11a, DSC analysis of the single I_2 phase gives a very small endothermic peak at 36 °C followed by an

(40) Doolittle, A. K.; Doolittle, D. B. *J. Appl. Phys.* **1957**, *28*, 901.
(41) Marshall, L.; Zukoski, C. F. *J. Phys. Chem.* **1990**, *94*, 1164.
(42) Panouillé, M.; Benyahia, L.; Durand, D.; Nicolai, T. *J. Colloid Interface Sci.* **2005**, *287*, 468.
(43) Kapnistos, M.; Vlassopoulos, D.; Fytas, G.; Mortensen, K.; Fleischer, G.; Roovers, J. *Phys. Rev. Lett.* **2000**, *85*, 4072.
(44) Rodríguez, C.; Shigeta, K.; Kunieda, H. *J. Colloid Interface Sci.* **2000**, *223*, 197.
(45) Durrschmidt, T.; Hoffmann, H. *Colloid Polym. Sci.* **2001**, *279*, 1005.
(46) Daniel, C.; Hamley, I. W.; Wilhelm, M.; Mingvanish, W. *Rheol. Acta* **2001**, *40*, 39.
(47) Rodríguez, C.; García-Román, M.; Kunieda, H. *Langmuir* **2004**, *20*, 5235.
(48) Princen, H. M. *J. Colloid Interface Sci.* **1983**, *91*, 160.
(49) Pons, R.; Erra, P.; Solans, C.; Ravey, J.-C.; Stébé, M. J. *J. Phys. Chem.* **1993**, *97*, 12320.
(50) Gradzielski, M.; Hoffmann, H.; Panitz, J.-C.; Wokaun, A. *J. Colloid Interface Sci*. **1995**, *169*, 103.
(51) Sollich, P.; Lequeux, F.; Hebraud, P.; Cates, M. *Phys. Rev. Lett.* **1997**, *78*, 2020.
(52) De Gennes, P. G. *J. Phys., Lett.* **1976**, *37*, L1−L2.
(53) Mallamace, F.; Chen, S.-H.; Liu, Y.; Lobry, L.; Micali, N. *Physica A* **1999**, *266*, 123.

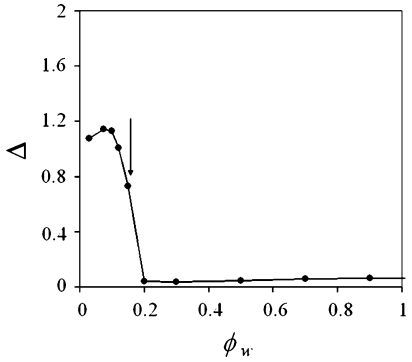

Figure 10. Exponent of the power law $G' \approx \omega^{\Delta}$ as a function of ϕ_w. The line is only a visual guide. The arrow indicates the onset of the disorder−order transition.

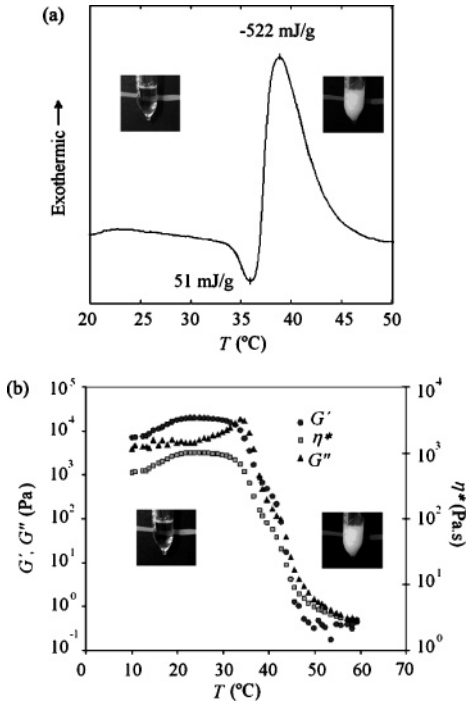

Figure 11. (a) DSC curve (heating) for a reverse micellar cubic sample. The water concentration is 20 vol %, and the $EO_5PO_{68}EO_5$/*p*-xylene weight ratio is 77/23. (b) Temperature ramp rheological test for the sample in (a). η^* is the complex viscosity, and G' and G'' are the storage and loss moduli, respectively. Test conditions are as follows: $\omega = 1$ Hz; stress = 6 Pa. The insets show the visual appearance of the samples below and above the transition temperature.

exothermic peak at 39 °C. The curves are different from those corresponding to other micellar organogels which show a glass transition.[45] The solidlike, transparent I_2 phase becomes fluid and turbid above 36 °C, as observed visually (see the insets in Figure 11). The turbidity comes from the macroscopic phase separation between a reverse micellar solution (resulting from the I_2 phase melting) and excess water. Therefore, the endothermic peak can be assigned to the melting of the cubic phase (order−disorder transition), whereas the exothermic peak comes from a phase separation process, which would be associated to a latent heat of demixing.[54] The melting process takes place in a relatively narrow range of temperatures, an indication of the presence of well-defined structures. The enthalpy associated with the melting transition is very small (51 mJ/g or 0.2 kJ/mol amphiphile) and is 1 order of magnitude smaller than the values found for direct micellar cubic phases,[47] in which the disruption of the hydrated structure of the hydrophilic groups facing the aqueous phase requires a higher enthalpy change. In reverse cubic phase liquid crystals, excluded volume effects represent the only kind of interaction among the aggregates. The value obtained for the enthalpy of transition (0.2 kJ/mol amphiphile) is of the same order of magnitude as those reported for thermotropic reverse discontinuous cubic phases[2,55] and organogels[56]

Figure 11b corresponds to a rheological temperature ramp test. The storage (elastic) modulus (G') prevails over the loss (viscous) modulus (G'') at low temperatures, indicating the solid character of the sample. G' approaches G'' as the temperature increases, and finally a crossover takes place at 36 °C. This indicates a decrease in the relaxation times as the temperature increases. The rise of G' between 10 and 20 °C might be associated with structural arrangement favored by both thermal and mechanical factors. The complex viscosity slightly increases with temperature but remains very high up to 36 °C and then suddenly drops, in agreement the melting process observed visually and by DSC. After the melting and phase separation processes, the sample behaves as a liquid, and therefore, $G'' > G'$. The results of Figure 11 are qualitatively similar to those obtained by Pouzot et al.[12] for the reverse micellar cubic phase in the monolinolein/water/limonene system, indicating a common signature of the order−disorder transition.

The preparation process of the reverse cubic phase-based emulsion can be explained by means of Figure 11. First, the mixture is heated above the melting point of the I_2 phase, so that the fluidity of the system facilitates the mixing. The sample is then cooled down to below the melting temperature, so that the I_2 phase is reformed around the droplets (see Figure 8), and a gel-like, concentrated emulsion is obtained.

Conclusions

Spherical reverse micelles are formed in poly(ethylene oxide)−poly(propylene oxide)−poly(ethylene oxide) (PEO−PPO−PEO) amphiphilic block copolymers in the presence of block selective solvents. These micelles swell with water and eventually pack in an ordered fashion, forming a reverse micellar cubic liquid crystal (I_2) having a *Fd3m* lattice and showing gel-like behavior with very high elastic moduli. The I_2 liquid crystal undergoes an order−disorder transition associated with endothermic (melting) and exothermic (phase separation) processes.

The reverse micellar cubic liquid crystal can act as a stabilizing external phase for water droplets, so that emulsions having a high internal phase ratio can be prepared. The elastic modulus and the viscosity of the emulsions decrease with the amount of dispersed water, but the emulsions remain gel-like up to high volume fractions of the dispersed phase. The results are helpful to understand the formation mechanism of reverse emulsions that might find use in several applications, including their role as templates. In fact, it was already found that reverse micellar cubic phases can also be formed using polymerizable oils such as divinylbenzene, which offers possibilities for the preparation of solid macroporous materials; results will be reported elsewhere.

Acknowledgment. This work was partly supported by Core Research for Evolution Science and Technology (CREST) of JST Corporation. C.R. thanks Josep Carilla (Institut d'Investi-

(54) D'Aprano, A.; Lizzio, A.; Liveri, V. T. *J. Phys. Chem.* **1987**, *91*, 4749.
(55) Kasten, H.; Stuhn, B. *Macromolecules* **1995**, *28*, 4777.
(56) Kleppinger, R.; Mischenko, N.; Reynaers, H. L.; Koch, M. H. J. *J. Polym. Sci., Part B: Polym. Phys.* **1999**, *37*, 1833.

gacions Químiques i Ambientals de Barcelona) for his help with DSC measurements. L.K.S. is thankful to the Ministry of Education, Culture, Sports, Science and Technology (MEXT) of Japan for the Monbukagakusho Scholarship. D.V. thanks JSPS for financial support. The authors are grateful to Dr. Takaaki Sato (Waseda University) for valuable discussions and comments on SAXS results.

Supporting Information Available: Freeze fracture electron microscopy image of a reverse micellar cubic phase, plot of the micellar core radius (r_c) as function of EO chain length in PEO−PPO−PEO block copolymer/water/*p*-xylene systems, and electron density profile of micelles at different volume fractions of water. This material is available free of charge via the Internet at http://pubs.acs.org.

LA701722F